Meteorol Atmos Phys (2007)
DOI 10.1007/s00703-006-0237-0
Printed in The Netherlands

Meteorology and Atmospheric Physics

[1] School of Meteorology, University of Oklahoma, OK, USA
[2] Cooperative Institute for Meteorological Studies (CIMMS), University of Oklahoma, OK, USA
[3] National Severe Storms Laboratory (NSSL), Norman, OK, USA

A high-resolution simulation of microphysics and electrification in an idealized hurricane-like vortex

A. O. Fierro[1], L. Leslie[1], E. Mansell[2], J. Straka[1], D. MacGorman[3], and **C. Ziegler[3]**

With 13 Figures

Received July 4, 2006; revised September 7, 2006; accepted September 17, 2006
Published online: March 21, 2007

Summary

Cloud-to-ground (CG) lightning bursts in the eyewall of mature tropical cyclones (TCs) are believed to be good indicators of imminent intensification of these systems. While numerous well-documented observational cases exist in the literature, no modeling studies of the electrification processes within TCs have previously been conducted. At present, little is known about the evolution of charge regions and lightning activity in mature TCs. Towards this goal, a numerical cloud model featuring a 12-class bulk microphysics scheme and electrification and lightning processes is utilized to investigate the evolution of the microphysics fields and subsequent electrical activity in an idealized hurricane-like vortex.

Preliminary results show that the highest total lightning flash rates (CG plus intracloud) are primarily found within the eyewall where updraft speeds tend to be larger than elsewhere in the TC, though rarely exceeding $10\,\mathrm{m\,s^{-1}}$. Smaller total flash rates are also found within the strongest cells forming the outer bands, where updrafts speeds sometimes reach $15\,\mathrm{m\,s^{-1}}$. As expected, these two regions of the storm are generally characterized by moderate total graupel mixing ratio ($\geq 0.5\,\mathrm{g\,kg^{-1}}$) and moderate cloud water content ($\geq 0.2\,\mathrm{g\,kg^{-1}}$). When the model uses the Saunders and Peck non-inductive (NI) charging scheme and moderate inductive charging settings, the inner eyewall region exhibits a complex charge structure. However, the charge regions involved in lightning can be described as a normal tripole charge structure while a normal dipole is observed in the outer eyewall stratiform region and in the strongest cells forming the outer rainbands. The charges forming the normal dipole in the outer eyewall are generated within the eyewall via NI charging in the mixed-phase region at mid-levels (near the $-10\,^{\circ}\mathrm{C}$ isotherm) and later are ejected radially outward by the storm's intense circulation.

1. Introduction

Tropical cyclones (TCs) are known for their destructive power, particularly as they make landfall. TCs often are accompanied by extreme winds, storm surges and torrential rainfall. Many populated coastal regions are threatened yearly by TCs and the 2004 and 2005 seasons were particularly active in the Atlantic basin. To improve forecasts of these storm systems it is important to acquire a better understanding of the internal dynamics of TCs.

With the advent of increasingly powerful computing resources, idealized numerical studies have successfully reproduced many of the main features of TCs that are observed in nature (e.g., Braun, 2002; Zhu, 2004). The availability of increasingly detailed observational datasets, many of which are derived from satellites, is crucial in initializing and verifying these numerical experiments (e.g., Velden et al, 1992). Previous modeling work has focused mostly on the large-scale

processes that control TC dynamics, and have led to significant progress in these areas (e.g., Emanuel, 1986, 1987; Zehnder and Reeder, 1997; Blackwell, 2000; Braun, 2002; Wang, 2002; Zhu, 2004).

In comparison, there have been relatively few modeling or model-related studies that have explored the microphysical processes in TCs (e.g., McFarquhar and Black, 2004; Rogers et al, 2006) and none of their electrification. Thus, little is known about these two physical aspects of the TCs, although better understanding of them may help improve short-term forecasts of their potential for severe weather, both at sea and at landfall. For instance, increasing total lightning flash rates (i.e., rates of intracloud plus cloud-to-ground lightning) indicates an increasingly large volume of graupel or small hail aloft, indicative of strengthening updrafts and an increased probability of heavier rainfall (e.g., Lhermitte and Krehbiel, 1979; MacGorman and Rust, 1989; Wiens et al, 2005). As a consequence, several observational studies have stressed the importance of a more systematic monitoring of any change in TC lightning flash rate particularly in the eyewall as an increase of the latter is often accompanied with an intensification of the storm (e.g., Lyons et al, 1989; Molinari et al, 1994).

The present study emphasizes increased knowledge of the microphysical and electrical structure of TCs as a significant, new step toward the development of the next generation of TC models. These kinds of models are a necessary part of a research effort aimed at improving model forecasts of hurricane intensity before and during landfall.

2. Current state of knowledge of electrification and microphysical processes in TCs

By using the cloud-to-ground (CG) lightning data from the National Lightning Detection Network (NLDN) for nine Atlantic hurricanes, Molinari et al (1999) delineated three distinct convective regimes in mature hurricanes: (1) the eyewall, which has attributes similar to those of deep, weakly electrified, monsoonal convection; (2) the region outside the eyewall (at about 90 km radius) that resembles the trailing stratiform region of mesoscale convective systems (MCS) (where MCSs tend to produce sparse, infrequent +CG strikes), and (3) the outer rainbands (at about 250 km radius), which contains the vast majority of the total number of ground flashes. Cecil et al (2002a, b) used the same convective regimes in a study of total lightning activity (intracloud plus cloud-to-ground flashes) in TCs.

For a TC to produce electrification strong enough to cause lightning, Black and Hallett (1999) showed that it must have an updraft magnitude large enough to produce both graupel and cloud liquid water in the mixed phase region (near the $-10\,^{\circ}$C isoform). This is true because the primary initial electrification mechanism in storms is a non-inductive (NI) exchange of charge between actively riming graupel and rebounding cloud ice particles, as found in laboratory studies by many investigators, including Takahashi (1978) and Saunders and Peck (1998). Black and Hallett (1999) observed that convective elements of hurricanes that produced riming graupel in the mixed phase region had significant electric field magnitudes, while elements that did not have graupel had no more than weak electric fields. The association of lightning with updrafts strong enough to produce riming graupel is consistent with observational (e.g., Lhermitte and Krehbiel, 1979; Wiens et al, 2005) and modeling (e.g., Mansell et al, 2005; Kuhlman et al, 2006; Fierro et al, 2006) studies of continental storms. In fact, these studies have shown that total lightning flash rates are correlated with updraft mass flux through the mixed phase region, with the volume of updraft $> 10\,\mathrm{m\,s^{-1}}$, and with graupel volume and mass.

Thus, one would expect electrification and lightning to be most likely in those parts of hurricanes that have the strongest updrafts. Black et al (1995) showed that graupel particles in deep, isolated eyewall convective cells of hurricane Claudette (1991) carried most of the negative charge at middle levels (near the $-5\,^{\circ}$C isotherm). In many TCs, however, charge generation in eyewall convection is limited by the liquid water content, as hurricane eyewalls contained relatively little supercooled water in much of the mixed phase region. For example, Black (1984) showed that little liquid water was found within the updrafts significantly above the freezing level in hurricanes Allen (1980) and Irene (1981). Furthermore, Black and Hallett (1986) showed that hurricane convection is often largely glaciated at temperatures as warm as $-5\,^{\circ}$C.

The sharp decrease in reflectivity with height within the eyewall and the inner rainbands further supports the notion that most of the liquid water carried above the freezing level by updrafts becomes frozen at altitudes below the $-10\,^{\circ}\mathrm{C}$ level. Jorgensen et al (1985) hypothesized that the rapid decrease of radar reflectivity and cloud water content above the freezing level could be attributed to an active warm-cloud coalescence process that would develop a full precipitating drop size spectrum before drops are lifted above the freezing level. As previously discussed by Kessler (1969, pp 4–6) for the case where fall-speed exceeds updraft speed, the larger drops would then fall out of weak updrafts and would leave many fewer drops to be carried into the higher level mixed phase regions. Jorgensen et al (1985) argued that this early fallout of the majority of the liquid water from the updraft before the particles freeze is consistent with a generally weak updraft ($<5\,\mathrm{m\,s^{-1}}$) near the melting level. Moreover, they argued that the large graupel often observed within the larger updrafts will accrete cloud water quickly leading progressively to complete glaciation of the cloud in the mixed-phase region (near $-10\,^{\circ}\mathrm{C}$).

Using trajectory analysis for the case of hurricane Emily (1987), Willis and Heymsfield (1989) argued that the ice particles growing and descending through the TC stratiform region are recycled from large reflectivity cores back into the lower levels of the eyewall. The high reflectivity values in the eyewall result from the fallout of graupel, raindrops and frozen drops close to their source. Willis and Heymsfield (1989) also hypothesized that the graupel is confined mainly to convective regions, but is active in secondary nucleation (i.e., via the Hallett-Mossop mechanism) to provide an abundant supply of ice crystals that become involved in aggregation outside the convective region. Furthermore, Black and Hallet (1986) argued that most of the ice content present in eyewall updrafts originates from the ''ice multiplication'' mechanism and is then redistributed throughout the storm by the upper- and mid-level anticyclonic circulations.

One other process that may limit the magnitude of electrical forces within some parts of TCs is the strong horizontal winds in those regions. Strong horizontal winds in the eyewall will tend to spread the charged particles horizontally over a broader area as differential sedimentation moves the microphysically-separated charges apart vertically to form macroscopic regions having significant net charge. The strong horizontal advection may limit the concentration of charge in the negative vertical wind gradient with height near the top of an updraft (e.g., as described by Ziegler et al, 1991) and, in any case, will separate the positive and negative charge regions farther from each other and thereby reduce the electric field magnitude.

Observations of lightning flashes that do not strike the surface in TCs are scarce, because there have been few ground-based systems capable of detecting a large fraction of cloud flashes and the range of such systems is typically only 100–200 km. Most such observations have been obtained from the lightning mapper on the Tropical Rainfall Measuring Mission (TRMM) satellite. Cecil et al (2002a, b) used aircraft observations during the TRMM field experiment to investigate intracloud (IC) and CG lightning activity and radar reflectivity patterns within the eyewall and the inner and outer rainbands of 45 hurricanes. They found that lightning flash rates in the eyewall and particularly within the outer rainbands were much greater than those within the inner rainband region. The inner rainband contains mainly stratiform precipitation and weak updrafts. This is consistent with the much weaker radar reflectivity observed above the freezing level within the inner bands. In contrast, the eyewall exhibits the greatest reflectivity values due to warmer temperature anomalies at mid-levels and the fallout of larger drops at low levels. Nevertheless, the reflectivity values and lightning activity still were much smaller than for continental storms. From these results, Cecil et al (2002b) inferred that supercooled water droplets are most plentiful within the outer rainbands.

Kelley et al (2004) suggested that having very deep clouds in the eyewall of TCs observed by the TRMM satellite was associated with a 70% likelihood of hurricane intensification. Such clouds would be more likely to produce lightning, so one might expect a relationship between increasing lightning flash rates and hurricane intensification. Unfortunately, most time-series observations of lightning in hurricanes during intensification have included only CG flashes that are essentially uncorrelated with updraft intensity and storm

severity, at least in continental storms (Reap and MacGorman, 1989). Though moderate to strong updraft speed through the mixed phase region is a necessary condition to produce the electrification needed by lightning, CG lightning also requires a charge configuration that will cause some lightning flashes to propagate downward to the ground. Several studies of continental storms (e.g., MacGorman et al, 1989, Carey and Rutledge, 1998) have shown that the probability of CG lightning increases with the formation and descent of precipitation to levels near or below the 0 °C isotherm and have suggested that precipitation is needed at lower levels to produce a small region of charge sufficient to initiate lightning downward in the middle to lower regions of the storm. Modeling studies demonstrate that a lower charge region opposite in sign to the main charge region is necessary for simulated CG flashes (e.g., Mansell et al, 2005; Kuhlman et al, 2006; Fierro et al, 2006).

However, several studies have found that CG flash rates increase during TC intensification, a useful correlation for forecasters particularly when monitoring a TC approaching landfall. Samsury and Orville (1994) analyzed lightning evolution for a weak TC (Jerry in 1989) and an intense TC (Hugo in 1989) within an 18 hour

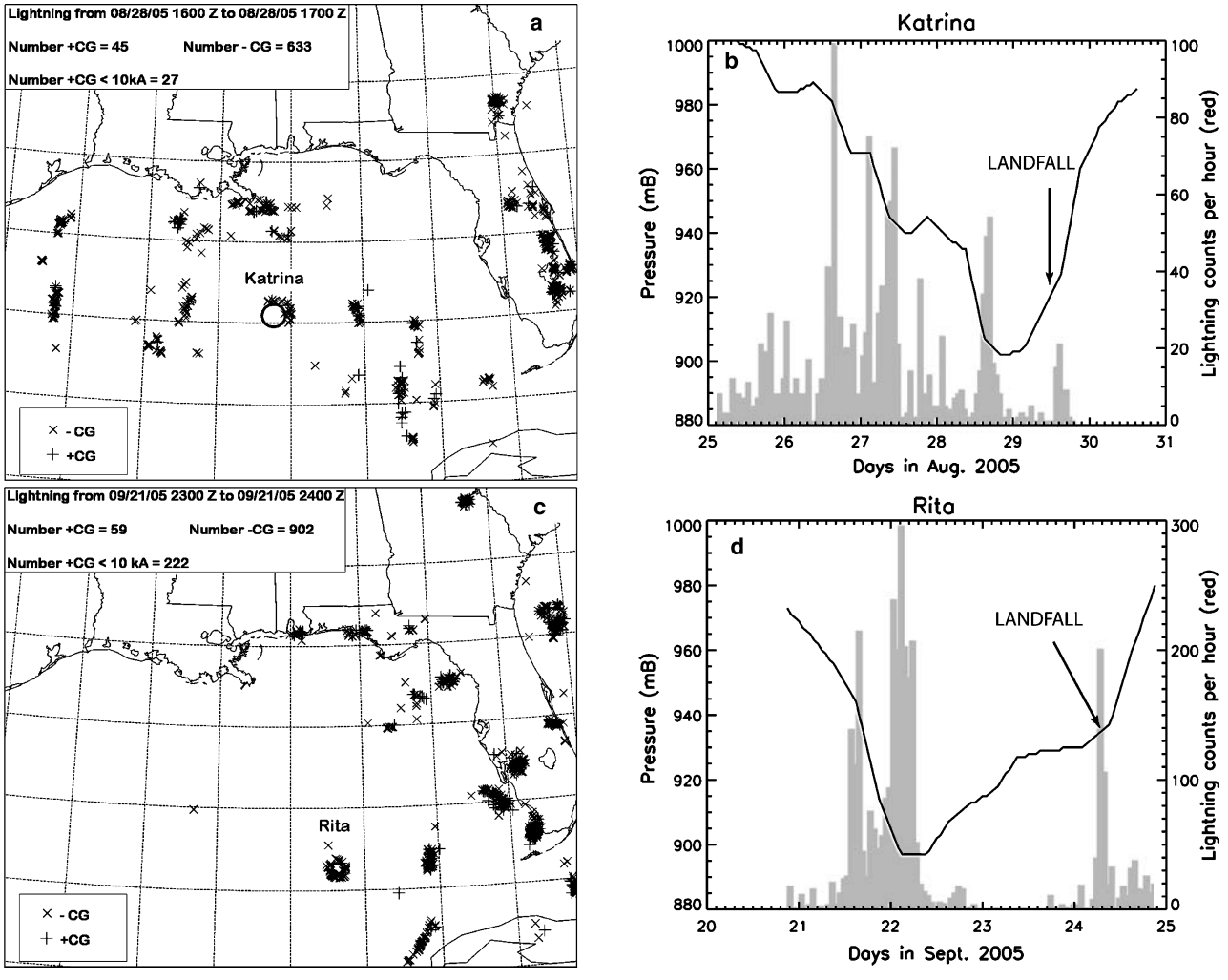

Fig. 1. Panels (**a**) and (**c**) show maps of CG lightning flash detected by the National Lightning Detection Network (NLDN) for an hour time period on the 28th of August for hurricane Katrina (2005) and on the 21st of September for hurricane Rita (2005), respectively. For both Rita and Katrina, a thick black circle depicts the approximate location of the storm's eye within that time frame. Panels (**b**) and (**d**) show time series of hourly eyewall total lightning flash rate detected by LASA (Los Alamos National Laboratory's Sferic Array) overlaid by NOAA central pressure for Katrina and Rita, respectively. The plots in panels (**b**) and (**d**) were provided by Dr. Xuan Min Shao from the Los Alamos National Laboratory in New Mexico. The results were presented by Shao et al, in the 2006 AMS meeting in Atlanta during a poster session

window that included the periods before and after the storm made landfall. They found that regardless of CG flash polarity, lightning occurs primarily within convective regions and is often associated with the largest radar reflectivity values. The correlation between the intensity of convection and reflectivity is consistent with the greater condensation rate of supercooled water in strong updrafts, as noted by Black and Hallett (1986). Orville and Coyne (1999) investigated the CG lightning flash characteristics in 34 TCs between 1986 and 1996. They found that as the TC became more organized, weak CG lightning activity occurred in the eyewall, while the minimum flash rates were observed in the inner stratiform rainband and the maximum flash rates were observed in the outer rainband. Rodgers et al (2000) found that the closer the lightning is to the storm's center, the more likely the TC is to intensify.

Demetriades and Holle (2005) used data from an experimental long-range CG lightning detection network to show that nine recent Atlantic hurricanes (such as Lili and Isidore in 2002, Isabel and Fabian in 2003, and Charley in 2004) experienced an outbreak of eyewall lightning in 11 of the 12 eyewall cycles present in those cases. Consistent with the observations of Black et al (1993) and Molinari et al (1999), these CG flash outbreaks tended to occur during the early intensification stage of the TC. Demetriades and Holle (2005) also supported the findings of Molinari et al (1999) that strong, mature, hurricanes remaining in a quasi-steady state showed weak or almost no lightning activity (e.g., hurricane Isabel in 2003).

Examples of lightning outbreaks, particularly within the eyewall, in recent hurricanes that intensified prior to making landfall in the US are shown in Fig. 1. (Most of the lightning flashes in the left panels of Fig. 1 were CG flashes, though the +CG flashes with peak currents less than 10 kA were probably cloud flashes (Cummins et al, 1998). Because cloud flashes tend to radiate weaker signals than CG flashes in the operating frequency band of LASA, the majority of flashes in the right panels also were CG flashes, though a substantial fraction may have been cloud flashes.) hurricane Katrina (2005, Fig. 1a, b) and Rita (2005, Fig. 1c, d) all exhibited similar trends, with flash rates increasing during TC intensification (Shao et al, 2005). These cases further suggest that eyewall lightning outbreaks might be a useful forecast tool to predict imminent changes in hurricane intensity and therefore to diagnose storm intensification.

As for continental storms (e.g., MacGorman et al, 1989), increasing CG flash rates can also accompany or precede a temporal weakening of weak TCs and/or an imminent change in its track (Willoughby, 1990). Furthermore, the strong relationship of cloud flash rates and total lightning flash rates (in contrast with the lack of relationship of CG flash rates) with updraft intensification means that systems that map all lightning would be preferable for monitoring the potential for intensification of TCs. Adding to the desirability of using such systems is the fact that cloud flashes typically outnumber CG flashes by a ratio of at least 2:1 (pp 190–192 of MacGorman and Rust, 1998; Boccippio et al, 2001), so lightning rate trends also will be sampled much better.

3. The numerical model and initialization procedures

The numerical model used in this study was developed by Straka and Mansell (2005) and solves the three-dimensional, non-hydrostatic, quasi-anelastic equations of motion (Anderson et al, 1985). Dimensional pressure and potential temperature are the prognostic thermodynamic variables, while temperature and density are diagnosed. The model uses a 1.5 order turbulence closure scheme where diffusion of scalars is based on the prognostic equation for the *square root* of turbulent kinetic energy (TKE) following Deardorff (1980). In total, 42 scalars are advected using a 6th order flux conservative Crowley scheme (Tremback et al, 1987) with a monotonic limiter (Leonard, 1991) on a forward time step. For velocity, an Asselin 1st-order leapfrog time scheme is used with a 6th-order (horizontal) local spectral scheme in space. A 2nd-order box scheme (quadratic energy conserving advection scheme) is used in the vertical for velocity.

The microphysical package in the model features 12 discrete, bulk hydrometeor habits with inverse exponential size distributions for all precipitation categories (Straka and Mansell, 2005). The distinct habits or categories are: cloud droplets, rain, cloud ice (columns, plates, and rimed),

snow particles, frozen drops, three graupel categories (each with a different assumed density), and two size ranges of hail. The interested reader may consult table 1 in Straka and Mansell (2005) for the parameters defining the different species. This wide variety of cloud particles is important when modeling cloud electrification processes, since it allows a wider spectrum of terminal fall speeds and differential fall speeds which in turn influence the magnitude of charge separated during single collisions. The model predicts mixing ratio of each category and diagnoses total concentration from mixing ratio and an assumed particle size. Cloud ice number concentration is diagnosed using the Meyers et al (1992) parameterization for the number of active cloud nuclei.

The electrification parameterizations available in the model are described by Mansell et al (2005). The primary electrification process in simulated storms is the non-inductive (NI) mechanism involving collisions between riming graupel and cloud ice. Among five NI schemes available as an option, the simulation reported in this study uses the Saunders and Peck (1998) NI scheme (hereafter referred to as SP98) which depends on the rime accretion rate (RAR) of graupel (Fig. 2). RAR is defined as the effective liquid water content (EW) multiplied by the differential fall speed V between the droplet and the graupel. EW is defined as cloud LWC times the collection efficiency of graupel for accreting cloud droplets. Brooks et al (1997) constructed a curve of critical RAR, which defines the upper and lower limit at which graupel acquires negative and positive charges, respectively. SP98 carried out further experiments at a larger range of temperature to better determine the RAR critical curve. In this study, the original SP98 curve has been modified by Mansell et al (2005) to be consistent with the fact that supercooled water can exist at temperatures as low as $-40\,^{\circ}\mathrm{C}$ and thus the curve has been translated towards that lower limit.

The model also features explicit treatments of small ions including attachment and drift motion following Chiu (1978). Additionally, corona emission, or point ion discharge currents, occurs at the ground whenever the magnitude of the vertical electric field component at a given point exceeds $5\,\mathrm{kV\,m^{-1}}$. Electrification via inductive or polarization charging is also allowed when hail and graupel collide with cloud water, as in Ziegler et al (1991). The inductive charging strength is determined by the rebound efficiency (R_{eff}) and average cosine of the angle of impact collision between the droplet and graupel particles (set to 0.40 degrees). Although the model also treats the inductive and NI collisional charging of hail following the same formulas as for graupel, the typically low concentrations of hail in storms (including the present TC simulation) limits the magnitude of hail charging relative to graupel charging.

In the lightning model (Mansell et al, 2002), bi-directional leaders are propagated in a stochastic step-like fashion on a constant resolution grid. The initiation of a lightning flash occurs when the ambient electric field at a given point in the storm exceeds the critical ''runaway'' threshold electric field. Charge is induced on the channel by the total electric field and is subsequently

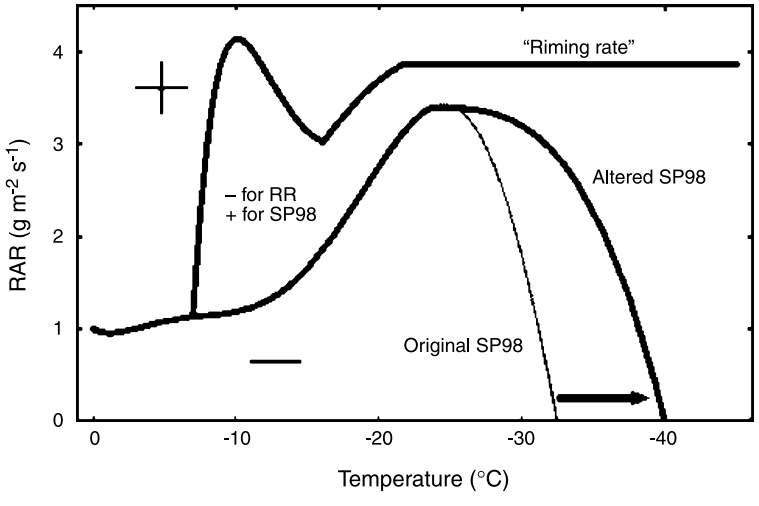

Fig. 2. Original Saunders and Peck (1998) and Riming Rate (Mansell et al, 2005) critical curves separating rime accretion rate (RAR) and temperature values at which a graupel particle gains positive charge from those at which it gains negative charge. Mansell et al (2005) altered the original SP98 critical curve as shown by the ''Altered SP98'' curve

released as small ions which can be captured by hydrometeors.

The initial wind field is imposed as a modified Rankine-type vortex in gradient wind balance (Kanak, 1990), the strength of which can be modulated via changes in its radius and maximum relative vorticity among other parameters. This modified Rankine vortex is cyclonic with radially and vertically decreasing intensity, and the vertical vorticity ξ is defined by

$$\xi = \left\{ \begin{array}{ll} \xi_{\max} & r = 0 \\ \xi_{\max} * \mathrm{e}^{-\alpha r^4} & 0 \le r \le r_{\max} \\ 0 & r > r_{\max} \end{array} \right\}.$$

$$\alpha = -\ln(0.1)/(r_{\max})^4 \qquad (1)$$

In the vortex initialization, the vorticity values are normalized on the horizontal plane by summing the vorticity values of Eq. (1), which is then divided by the sum of $\sin(\pi * r/r_{\max})$. The resulting ratio is then multiplied by each value of the sine function, which is then subtracted from each value of (1) to achieve a vorticity field with equal amount of positive and negative vorticity. The wind field is then computed using the streamfunction Φ defined as

$$\begin{aligned} \nabla^2 \Phi &= \xi, \\ u &= A \frac{\partial \Phi}{\partial y}, \\ v &= A \frac{\partial \Phi}{\partial x}, \end{aligned} \qquad (2)$$

where A is a function which forces the winds to decrease exponentially in the vertical and is defined as

$$A = \left\{ \begin{array}{ll} 1 & \mathrm{z} \le 15\,\mathrm{km} \\ \mathrm{Exp}\left(-\left(\frac{\mathrm{z}-15}{2}\right)^2\right) & \mathrm{z} \ge 15\,\mathrm{km} \end{array} \right\}. \qquad (3)$$

For our idealized simulation we chose $\xi_{\max} = 13 \times 10^{-4}\,\mathrm{s}^{-1}$ and $r_{\max} = 280\,\mathrm{km}$. With these settings the maximum winds are about $43\,\mathrm{m\,s}^{-1}$ and are located at a distance of 180 km from the center (Fig. 3). If the initial winds were to be weaker, a significant delay in the development of the convection by frictional convergence would occur, and in some cases, a hurricane-like vortex would fail to form. This procedure was mainly motivated because of the large amount of CPU needed for this hurricane simulation. On the other hand, initial winds greater than about $55\,\mathrm{m\,s}^{-1}$ with the same initial vortex radius would cause rapid development of scattered convection throughout the domain. In the latter case, widespread convection ultimately dominates the eyewall convection, resulting in an early decline of the storm.

The TC simulation was carried out on an *f*-plane with a constant Coriolis parameter set to $3 \times 10^{-5}\,\mathrm{s}^{-1}$. We did not consider latitudinal variations of *f*, since the latter mainly influences the storm track rather than the storm microphysical and electrical structure. Indeed, Fiorino and Elsberry (1989) found that the linear beta term is responsible for the formation of an initially asymmetric east-west oriented dipole structure called ''beta gyres''. Later, the nonlinear advection of the asymmetric circulation by the symmetric vortex reorients these gyres in a NE–SW fashion, causing a so-called ''ventilation flow'' towards the NE rather than towards the south. This rotation of the gyres occurs because the nonlinear advection is in balance with the linear beta forcing. This ventilation flow causes TCs in the northern hemisphere to drift towards the north while the mean steering current is towards the west.

Simulations with lower values of f (i.e., $< 2 \times 10^{-5}\,\mathrm{s}^{-1}$) were nearly similar to runs carried out with *f* set to zero. Early test runs revealed that setting $f = 0$ resulted in intense convection that developed rapidly around the eyewall, and led to a rapid demise of the TC. Moreover, as f increases the diameter of the eyewall increases as additional supply of planetary vorticity is constantly ingested into the storm, acting has an additional source of angular momentum. The surface pressure at sea level is 1011 mb everywhere across the domain. The sea surface temperature was set to 28 °C to enhance surface sensible heat fluxes at the lower boundary or first grid point above the ground of the domain. The surface layer parameterization makes use of velocity dependent, bulk aerodynamic formulae for sensible and latent heat fluxes, as well as for momentum fluxes following Rotunno and Emanuel (1987). The model also uses the surface dissipative heating parameterization of Bister and Emanuel (1998). The primary reasons for using these more simplistic bulk aerodynamic formulae (compared for example to the Louis 1979 surface layer parameterization) is that we use a rather coarse

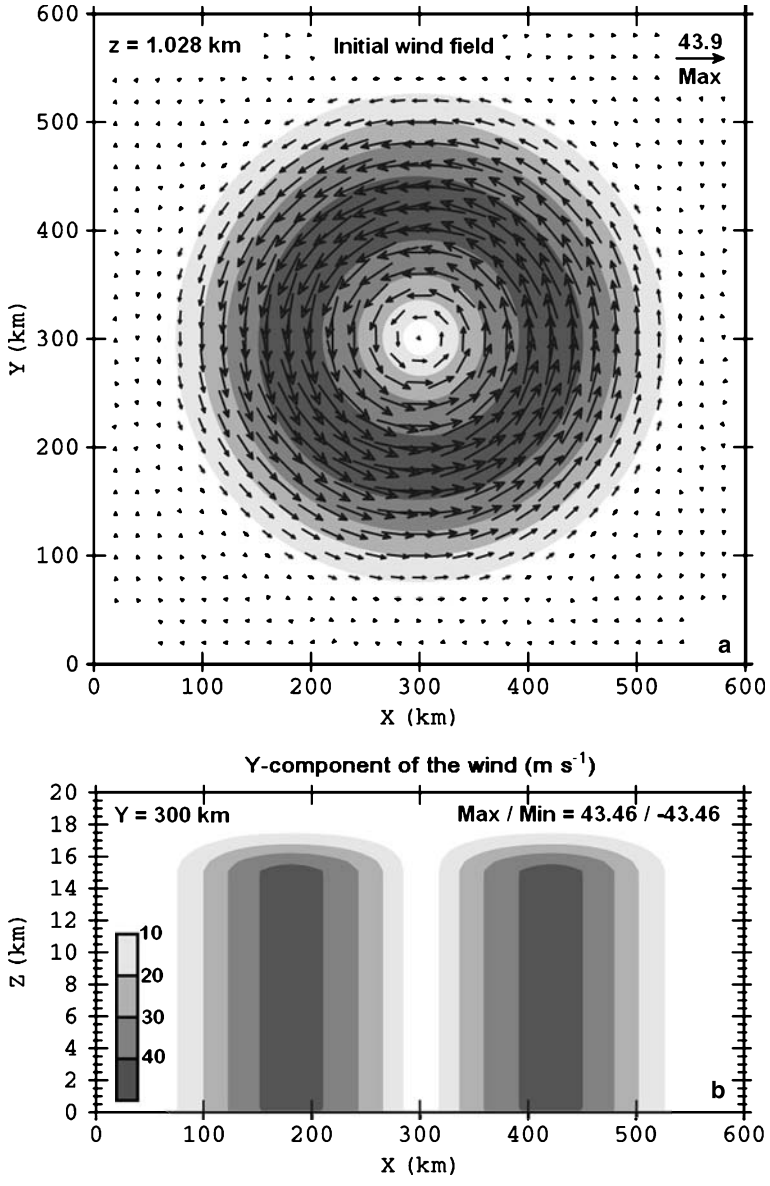

Fig. 3. Horizontal cross section of the initial wind vector field overlaid by the initial wind speeds at $z = 1.028$ km, and (**b**) vertical cross section (X–Z) at $Y = 300$ km of the initial wind speed. The wind speed scale for both panels is shown in panel (**b**)

resolution in the vertical and also because they are valid for high wind speeds. Also, they are very easy to implement and have been tested with success for hurricane simulations with somewhat coarse vertical resolution by Rotunno and Emanuel (1987).

The simulation presented in this study was carried out in a domain having horizontal dimensions of 300×300 and 46 vertical levels with a horizontal grid spacing of 2 km on an Arakawa C-grid. The vertical grid stretches from 200 m at the surface to a constant value of 600 m between 5.5 km and 17 km AGL. Above 17 km, the vertical grid stretches from 600 m to 1200 m. The lightning grid spacing was set to 1 km.

The initial horizontally homogeneous environmental profiles were represented by a composite of the 00 UTC Owen Roberts Airport, Grand Cayman Island sounding below $z = 15$ km km with the 00 UTC Kingston, Jamaica sounding of August 13th 2004 above 15 km (i.e., black thicker line in Fig. 4). The compositing was done because at that particular time, the Grand Cayman Island sounding had no data above 15 km. The Kingston sounding was chosen for the composite since it was the closest station available around the Grand Cayman Island. Hurricane Charley passed over or near the islands (less than 100 miles) near the time of the soundings and was rated as a category 3 on the Saffir-Simpson scale

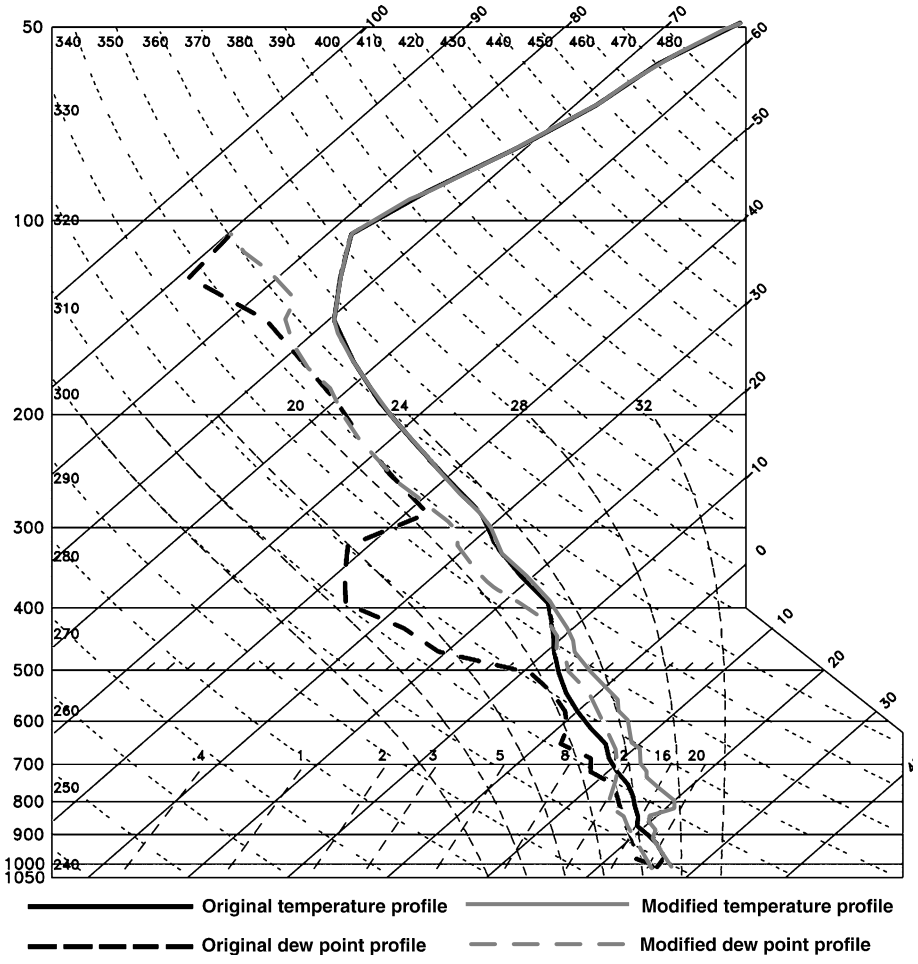

Fig. 4. Original (modified) composite Skew-T log-p diagrams shown in thick black (grey) lines for original (modified) sounding of the 13th August 2004, 00UTC Owen Roberts Airport, Grand Cayman Island and 00 UTC Kingston, Jamaica

(Simpson, 1974). As shown by the gray thicker lines in Fig. 4, the original composite sounding was modified in order to optimize the chances for a well defined hurricane-like vortex to form. The dry layer present between 300 and 500 mb is likely a residual Saharan airmass (Jason Dunion, personal communication, 2006). Since this layer does not have a maritime tropical origin and since its presence would weaken the simulated TC, it was removed from the sounding. The sounding was also moistened between 500 and 800 mb to reduce evaporative cooling and hence downdraft strength at these levels (e.g., following results of storm-scale simulations of Gilmore and Wicker, 1998). Also, between 700 and 850 mb, a capping inversion layer was added to prevent the convection within the bands from developing too rapidly at the beginning of the simulation. After these modifications, the sounding is nearly moist adiabatic, which is what is typically observed in the tropics over ocean away from land. The CAPE and CIN values of the model sounding (i.e., when interpolated to the model grid) were about 1474 and 99 J kg^{-1}, respectively, compared to 1560 and 22 J kg^{-1} in the original composite sounding.

It is noted that due to the idealized nature of the hurricane initialization in the model, the simulation presented in this study is not intended to reproduce hurricane Charley (2004). Rather, the environmental conditions from this sounding are believed to offer an initial field that would favor hurricane development in the model. That is, the sounding is assumed to be representative of typical conditions nearby intensifying or steady state hurricanes over ocean.

4. Results

4.1 Early evolution of the simulated TC

The simulated vortex went through several phases, the first phase being the rapid development of convection in concentric rings around the center

at about 2.5–3 h (not shown) which was partly caused by using a homogeneous environment as the initial condition. As time progressed, the individual convective elements organized around the center to form a broad ill-defined eye around 9–10 h, coincident with a rapid increase of the areal coverage of the storm (e.g., in terms of the 40 dBZ reflectivity contour at 1 km AGL) and a progressive decrease in minimum surface pressure (not shown). After about 10 h, the eyewall began shrinking due to advection and conservation of angular momentum from the induced secondary circulation. Schubert and Hack (1982) found that the contraction of a cyclonic vortex may also result from heating by convection inside a region of strong inertial stability. By about 19 h of simulation, the hurricane vortex reflectivity pattern exhibited several observed features of mature hurricanes, including a more solid, narrow ring of strong convection around the storm's center or eye and the formation of several spiral rainbands around the eyewall. Clearly, the early development stage of the storm was unrealistic, since convection was forced via frictional convergence by using a quasi–symmetric Rankine type vortex already having category 1 hurricane force winds embedded in a homogeneous environment (Fig. 4).

The total simulated lightning activity, particularly the IC and −CG flash rate was correlated with the storm total 35–40 dBZ areal coverage (not shown). The area of 35 dBZ radar reflectivity reached a maximum radius of about 200 km at about 10 h of simulation. Around that time, IC flash rate exceeded 1000 flashes per minute, which may be unrealistically high. Later on, however, as the intense ring of convection around the storm center shrank to more realistic sizes (10–15 km radius at about 20 h), the total IC flash rate decreased below 400 flashes per minute, which may be closer to actual values (although no reliable IC flash rate data are yet available for mature hurricanes over ocean).

Between 20 and 24 h (not shown), the eyewall convection shrank further, and the updraft speeds just above the melting level ($z = 6.1$ km AGL) showed a clear general weakening trend. The rainband convection, on the other hand, gained strength and increased in areal coverage. Updraft speeds of $5\,m\,s^{-1}$ and greater were found all around the eyewall at that time. At about 28 h, however, eyewall updrafts speeds rarely reached $5\,m\,s^{-1}$, while the eastern portion of the eyewall was dominated by weak downdrafts ($1\,m\,s^{-1}$) at this level. The exact reasons for this rapid weakening of the eyewall updraft mass flux are not clear and will be addressed in the future work section in more detail.

4.2 Early mature TC structure (21 h 40 min)

As previously described, the simulated vortex experienced several phases and for this reason a common slice time was selected for analysis of the results. The vortex started to resemble a mature hurricane near 20 h and therefore, a common slice time of 1300 min (21 h 40 min) was chosen. At that time, the minimum surface pressure was about 949 mb and the eyewall updraft was generally characterized by high equivalent potential temperature (θ_e) values of about 360–365 K (Fig. 5), which are almost 10 K higher than the values proposed by Gray (1995). Relatively higher θ_e values ranging between 360 and 365 K were

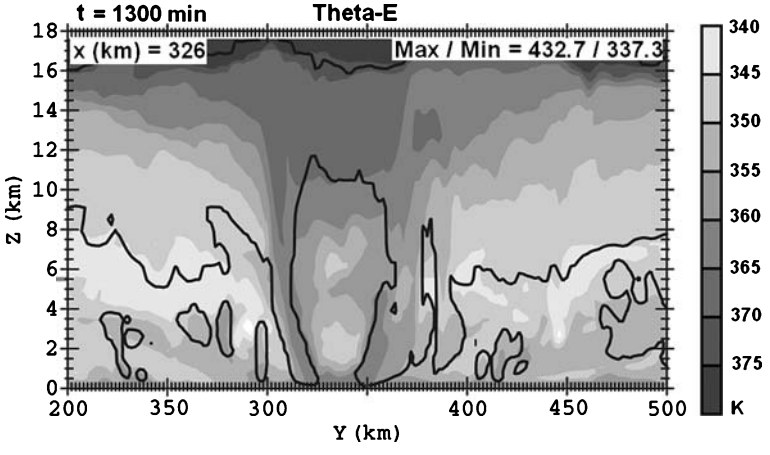

Fig. 5. Vertical cross section in the Y–Z direction at $X = 326$ km of cloud mixing ratio ($0.1\,g\,kg^{-1}$ contour in thick black line) and equivalent potential temperature (indicated by shading). Note that the maximum altitude on the vertical axis goes to 18 km, instead of 20 km for all remaining model cross sections shown in this study

found below 1 km AGL in the eye compared to values of about 345–350 K just above that level, consistent with observations (e.g., Gray, 1995). This sharp θ_e gradient of about 20 K in the eye near 1 km is associated with the observed inversion separating the more humid, warm air in the boundary layer caused by moist air inflow from the drier air from aloft that has been trapped by the TC circulation (similar to observations made by Willoughby, 1998). However, Willoughby (1998) found that this inversion was generally located at higher levels between 850 and 500 mb. Above 8 km in the eye, θ_e steadily increased to values ranging between 365 and 370 K near 13 km AGL (Fig. 5), due to adiabatic compression, and hence warming, of subsiding air in the eye.

The eyewall convection and resulting radar reflectivity exhibited a noticeable asymmetry (Fig. 6), as is often the case for mature hurricanes in nature. Tangential wind speeds exceeded 60 m s^{-1} (not shown), with the highest gusts just within the boundary layer above the surface (Fig. 7). Thus, the simulation corresponded to a mature high-end category 3 storm at this time. Consistent with many *in situ* aircraft observations, the simulated TC eyewall tangential winds exhibited an outward tilt with height (Fig. 7),

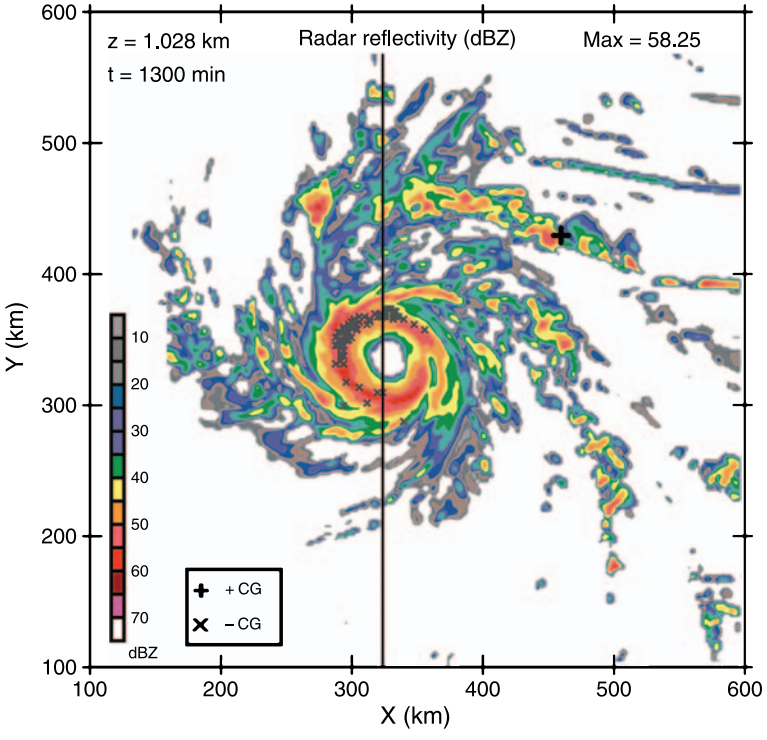

Fig. 6. Horizontal cross section of radar reflectivity (dBZ) at t = 1300 min and z = 1028 km. Shading indicates reflectivity in 5 dBZ increments from 5 to 75 dBZ. Locations of CG lightning strikes are also shown by a cross for −CG flashes and by a + for +CG flashes. The flash locations were plotted for a 30 min interval up to the cross section time. A black line shows the location of the vertical cross section of the majority of the plots shown in this study

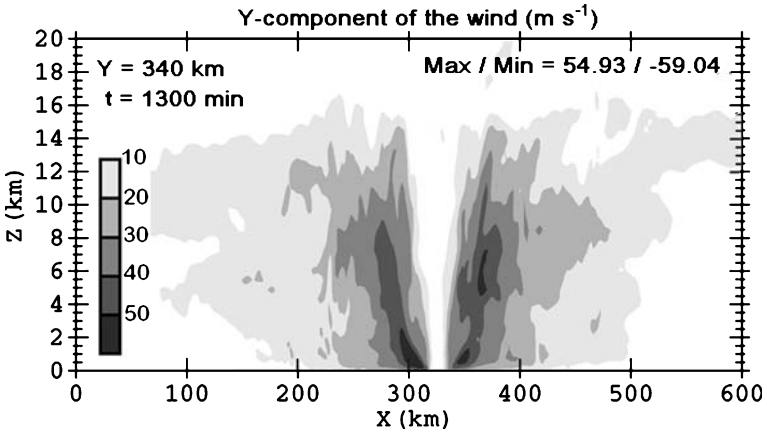

Fig. 7. X–Z Vertical cross section at Y = 340 km of the Y-component of the wind. Shading indicates the Y-component in 10 m s^{-1} increments

also seen in the vertical reflectivity profile (Fig. 8a). Between the eyewall and rainband convection, a stratiform region with weak reflectivity values was also evident (e.g., see Fig. 8a at Y = 390 km). Secondary weak bands below the outer core stratiform region of the eyewall were also found on the western and eastern flanks of the storm (see Fig. 8a at Y = 400 km). The heaviest rainfall occurred in the vicinity of the eyewall, with a secondary maximum in the outer rainband (Fig. 8a).

It is well-established from satellite observations that hurricanes tend to exhibit considerable variations in their size and shape. The overall eyewall vertical reflectivity profile of intense hurricanes (i.e., category 3 or greater), however, do exhibit more consistent similarity. Therefore, a comparison of the simulation with airborne radar measurements of hurricane Emily in 2005 (category 4 at the time of the scan) can be made. The NASA ER-2 airborne Doppler radar (EDOP, Heymsfield et al, 1996) observations from the Tropical Cloud Systems and Processes (TCSP, Halverson et al, 2006) field program shows noticeable similarities in the eyewall convection with the simulated TC. For instance, the 35 dBZ contour reaches up to about 10 km in the observations and to about 11–12 km in the simulation (Fig. 8a, b). However, hurricane Emily (2005) was extreme in terms of convective and electrical activity with electric fields as large as 9 kV m^{-1} measured above that storm. This is the highest value ever recorded above a TC (Dr. Blakeslee, personal communication, 2006). To highlight the rarity of such an event, the reflectivity profile across the eyewall of hurricane Katrina (2005) reveals that the 33 dBZ echo top hardly reached 7 km in the eyewall (Robert Rogers, personal communication, 2006). Another more contrasting example is hurricane Isabel (2003), which showed even weaker reflectivity values in its eyewall (J. Gamache, personal communication, 2006). The weaker reflectivity values may explain why, unlike Katrina, Isabel was overall

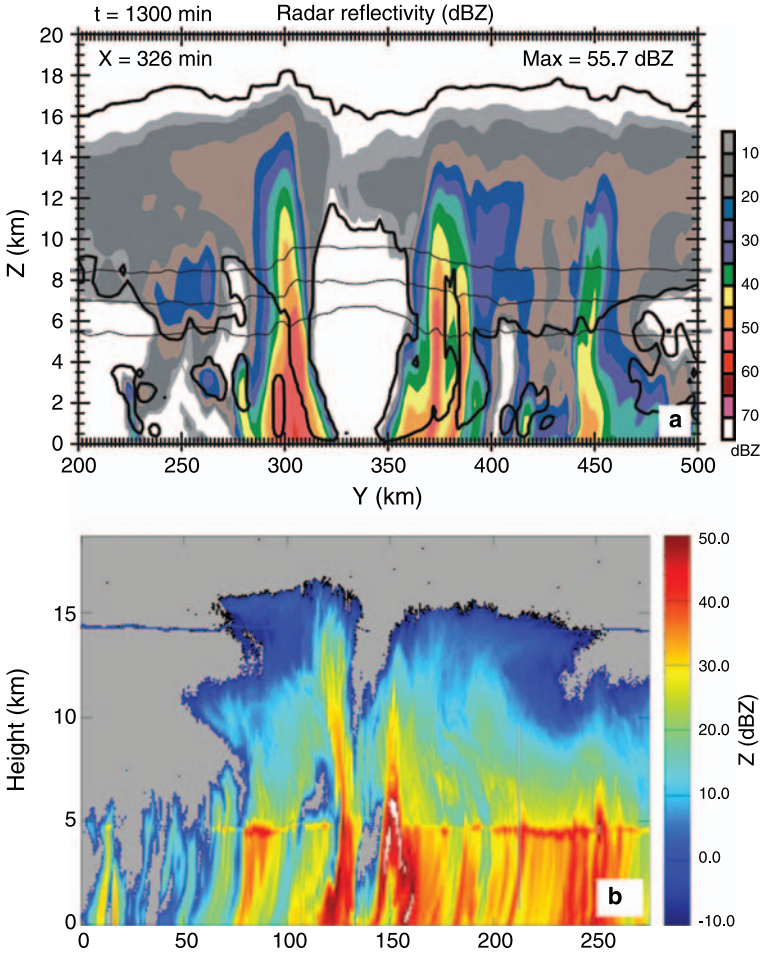

Fig. 8a. Radar reflectivity in the vertical cross section across the eyewall in at X = 326 km. Shading are as in Fig. 6. Panel (**a**) shows only a section of the total Y domain distance from 200 km to 500 km The quasi-horizontal thin black lines represent isotherms at 0, −10 and −20 °C, which represent the portion of the mixed-phase region in which most of NI charging occurs. The thick black contours are for cloud mixing ratio of 0.1 g kg^{-1} which depicts the cloud boundary. Panel (**b**) shows radar reflectivity from a NASA ER-2 Doppler Radar (EDOP) overflight of hurricane Emily on the 17th of July 2005 between 8h33–8h57 Z when the hurricane was a category 4. The data were collected by the EDOP during the Tropical Cloud Systems and Processes (TCSP) field program in 2005

devoid of lightning activity in its eyewall during its steady-state period as a category 5 storm (Molinari et al, 1999; Demetriades and Holle, 2005).

For both this simulation and for hurricane Emily (2005), the maximum height of detectable reflectivity values lies near z = 16 km. In the simulation, however, no clear evidence of a well-defined inner band (Cecil et al, 2002a) stratiform region was found between the outer rainbands and the eyewall. The reflectivity values there were rather small (i.e., <30 dBZ) below the melting level compared to the reflectivity values of hurricane Emily (Fig. 8a at X = 420 km and Fig. 8b at X = 170 km). In the model, the fallspeed of small ice crystals and snow particles are single-values functions of mixing ratio and fall at speeds ranging between 1 and 1.5 m s^{-1}, respectively. Therefore, these ice particles melted and evaporated quickly before reaching the ground and produced the weak reflectivities below the melting level in the inner band region of the simulated TC.

A radar-indicated bright band was clearly visible in hurricane Emily (2005, Fig. 8b) and located the melting level near 5 km. This level, however, was in good agreement with the temperature profile of the simulation (melting level located near 5.5 km, Fig. 8a). On the other hand, the simulated TC does not reproduce a bright band, possibly due to not predicting particle concentrations as done by Zrnic et al (1993).

Overall, the simulation tended to produce larger reflectivity values than the observed cases. Such differences were also noted by Rogers et al (2006) in their high resolution (1.67 km) numerical simulation of hurricane Bonnie (1998) and Floyd (1999), using the MM5 numerical model. Their composite analysis of precipitation radar (PR) reflectivity data from 34 passes across 18 TCs and tail Doppler radar data from 233 legs across 9 TCs revealed that the eyewall reflectivity rarely exceeded 40 dBZ below the 5 km level, while the model tended to produce reflectivity values exceeding 55 dBZ there. They hypothesized that this was likely caused by inadequacy of reflectivity-mass (Z–M) relationships in the calculation of reflectivity in the model, uncertainties in the assumption of the hydrometeor fall speeds used to compute the vertical motion of the air, and possible differences in resolution between observational and model data. It is speculated herein that the inability of the current 1-moment microphysical parameterization to treat snow aggregation (as in the 2-moment scheme of Zrnic et al, 1993) is another source of possible model error.

Just above the melting level at about 6.1 km, updrafts speed in the simulated eyewall rarely exceeded 10 m s^{-1}, while updraft magnitudes exceeding 5 m s^{-1}, however, were fairly common in the simulated eyewall within the mixed phase region (defined as the layer between the 0 °C and −20 °C isotherm between about 5 and 7 km, Fig. 9a, b), which should be adequate for sufficient electrification to occur (Black and Hallett, 1999, Petersen et al, 1999). Updraft magnitudes exceeding 5 m s^{-1} were also found at higher levels near 9 km in the simulation (not shown), and this further supports the likelihood of significant electrification occurring there. The same is true within some of the individual cells forming the rainbands, where isolated updrafts sometimes exceeded 15 m s^{-1}. The eastern portion of the eyewall was dominated by downdrafts and weak reflectivity values (Figs. 9a and 6). Overall, the eyewall was dominated by updrafts, consistent with Jorgensen et al (1985) and Rogers et al (2006). The presence of downdrafts on the outer edges of the eyewall updrafts was also consistent with observations (Fig. 9b).

However, the overall updrafts speeds shown in Fig. 9b are generally greater than those observed in real hurricanes. Rogers et al (2006) showed that vertical velocities obtained from vertical incidence tail Doppler radar data from 233 radial legs from 9 different TCs were generally weak ($|w|<2$ m s^{-1}) with only 1–2% of these exceeding a magnitude of 6 m s^{-1} (with extreme localized events reaching 12 m s^{-1}). These results were in agreement with Black et al (1996) who found that in seven Atlantic hurricanes, 70% of the vertical velocities ranged from −2 and 2 m s^{-1} while only about 5% exceeded 5 m s^{-1}. Such extreme events were observed for instance in hurricane Emily (1987, Black et al, 1994) and hurricane Katrina. Updrafts speeds exceeding 8 m s^{-1} (6 m s^{-1}) were found at 4 km (12 km AGL) in hurricane Katrina's eyewall as it reached category 5 status on the 28th of August 2005 near 1800Z (Robert Rogers, personal communication, 2006).

After about 15 hours of simulation, the updraft speeds in the eyewall experienced a general

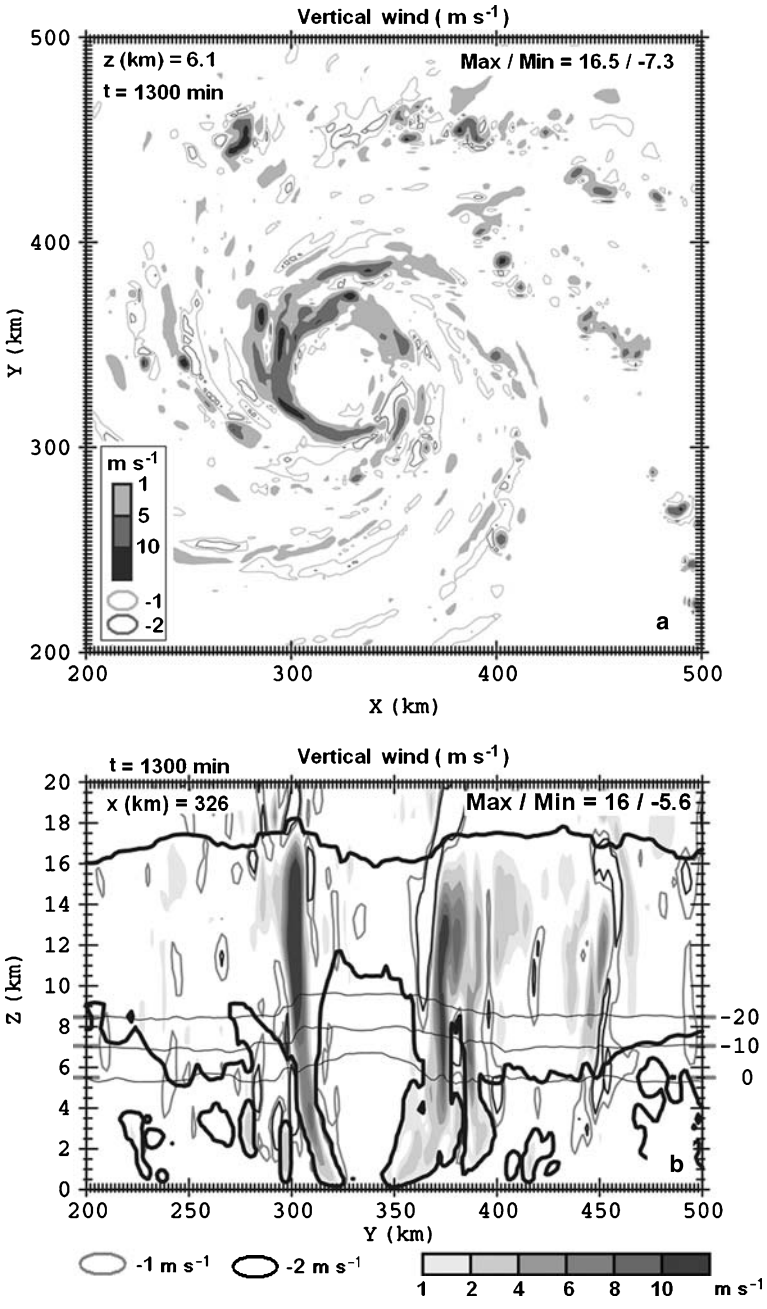

Fig. 9a. Vertical winds indicated by shading in a horizontal cross section at $z = 6.1$ km just above the melting level, and (**b**) a vertical cross section through the eye at the same location as in Fig. 8a. The thick black contours and thin black lines in panel (**a**) have the same meaning as in Fig. 8a

weakening trend until the eyewall convection started to dissipate after 35 hours of simulation time. This weakening of the eyewall convection will be discussed later in this section. Similar cross sections across the eye at later times (e.g., 25 hours), showed more realistic, weaker vertical winds in the eyewall along with smaller (and maybe more realistic) mixing ratios of heavier hydrometeor species, such as graupel (not shown). This in turn resulted in overall weaker reflectivity values at all levels and weaker total lightning activity in the eyewall. Despite the results being quantitatively different between 21 and 25 hours, the qualitative aspects of the storm remain unchanged and thus, any detailed analysis of the storm's dynamical, microphysical and electrical properties carried out in this time window will be similar.

4.3 Simulated TC microphysics and electrification

Moderate total hail ($\geq 0.2\,\mathrm{g\,kg^{-1}}$) and total graupel ($\geq 0.5\,\mathrm{g\,kg^{-1}}$) mixing ratios were found primarily within the eyewall and within the individual

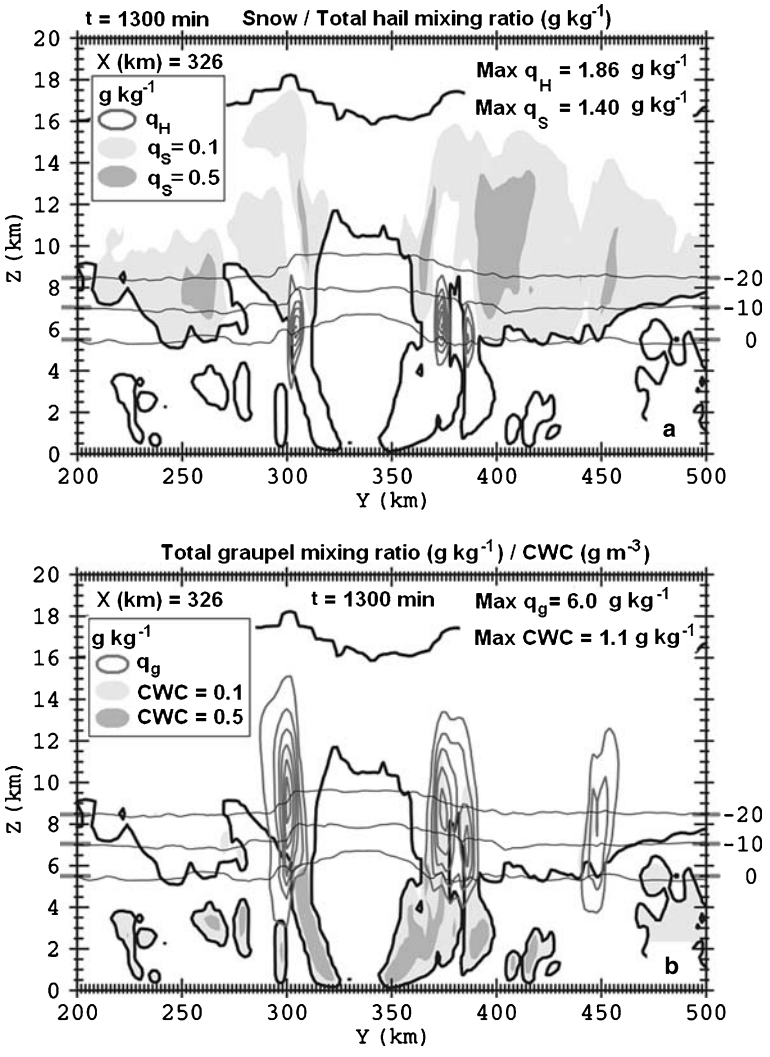

Fig. 10. Vertical cross sections in the Y-direction at $X = 326\,\mathrm{km}$ and $t = 1300\,\mathrm{min}$ (**a**) for snow mixing ratio and total hail mixing ratio, and (**b**) for total graupel mixing ratio and cloud water content (CWC in $\mathrm{g\,m^{-3}}$). Total mixing ratios are the sum of the mixing ratios of all the graupel (small, medium, and large) and hail (small, large) categories. The black thick line depicts the cloud boundary ($0.1\,\mathrm{g\,kg^{-1}}$ cloud mixing ratio). Legend for shadings and contours are shown in each panels. The total graupel (hail) mixing ratio contours are shown by increments of $0.3\,\mathrm{g\,kg^{-1}}$ ($1.0\,\mathrm{g\,kg^{-1}}$)

convective cells forming the outer rainbands (Fig. 10). The lighter ice crystals and snow particles nucleating inside the eyewall were advected radially outward by the strong TC circulation to form a large anvil cloud (Fig. 10a at $X = 390\,\mathrm{km}$). Hail particles were found near the $0\,^{\circ}\mathrm{C}$ and $-10\,^{\circ}\mathrm{C}$ isotherms (Fig. 10a), while the majority of the smaller, lighter graupel pellets were located further aloft in the eyewall updraft between the $-10\,^{\circ}\mathrm{C}$ and $-20\,^{\circ}\mathrm{C}$ isotherm (Fig. 10b). The majority ($>90\%$) of the graupel present there consisted of moderate and high density graupel, while low density graupel particles were rare and were found mainly at higher altitude near 12 km (not shown). As expected, these hydrometeors were located near moderate to strong updrafts (Figs. 9b, 10) which were also associated with larger cloud water content (CWC) due to enhanced condensational heating and thermal buoyancy forcing.

Since the eyewall and the strongest cells forming the rainbands contained the largest mixing ratios of graupel ($\geq 0.5\,\mathrm{g\,kg^{-1}}$) and the larger CWC ($\geq 0.2\,\mathrm{g\,m^{-3}}$) and updrafts, these regions were more conducive for collisional NI charging processes to operate between graupel or hail and the lighter ice crystals. Consequently, these regions also produced the largest flash rates in the TC (compare Figs. 10 and 11). At the time shown in Fig. 11, the IC flash rate of the entire storm system was about 300 per minute (not shown). However, based on Figs. 11 and 12 alone, it was not possible to distinguish which fraction of this total lightning activity occurred within the eyewall and within the outer rainbands of the storm. A simple analysis of horizontal and vertical cross

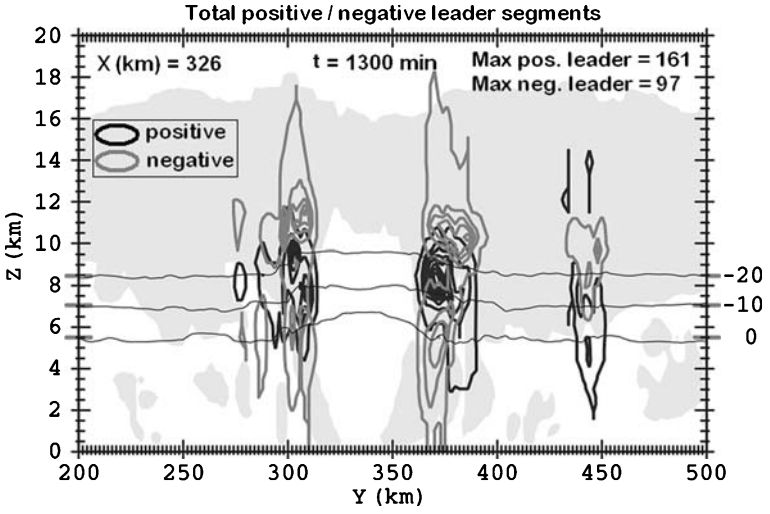

Fig. 11. As in Fig. 10, but for cloud mixing ratio $\geq 0.1\,\mathrm{g\,kg^{-1}}$ (grey shaded area) and positive (negative) leader segments in black (darker grey) contours. The contours show the horizontally integrated sum of positive or negative leader segments at each level in the domain for a period of 30 minutes prior to the cross section time (i.e., number per level per 30 minutes). The total leader contours are shown by increments of 20. The contour representing a total of one leader is also shown

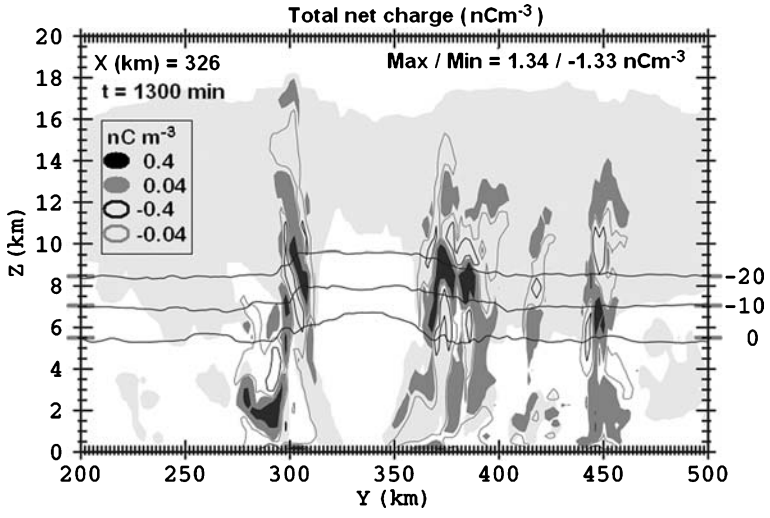

Fig. 12. As in Fig. 10, but for the total amount of net charge in $\mathrm{nC\,m^{-3}}$. Dark grey (black) shaded areas show region where net charge exceeds 4×10^{-2} ($0.4\,\mathrm{nC\,m^{-3}}$). Likewise dark grey (black) contours show where negative net charge magnitudes exceed 4×10^{-2} ($0.4\,\mathrm{nC\,m^{-3}}$)

sections (i.e., Figs. 6 and 11) indicated, however, that around the time of the figure, the majority of the total lightning flashes (i.e., all IC and CG flashes) was found in the eyewall. These lightning flashes in the eyewall were found to initiate in two distinct layers, approximately between 6 km and 8 km and between 9 km and 11 km. These layers coincided with the interfaces between regions of net positive charge and negative charge (Fig. 12), where the electric field magnitude was largest.

Several vertical cross sections taken in slightly different locations across the eyewall revealed small to moderate differences in charge structure and magnitudes. The overall charge structure in the eyewall and the rainbands was more complex than simple normal dipoles (positive charge above negative charge) or normal tripoles (composed of a normal dipole with a lower positive charge) commonly found in the literature (e.g., Williams, 1989). Indeed, the charge polarity in these two convectively active regions of the TC switched several times versus height and was composed of many pockets of weaker (i.e., $< 0.4\,\mathrm{nC\,m^{-3}}$) charge density (Fig. 12). Broadly, considering only the charge regions involved in lightning (i.e., regions with charge density $\geq 0.4\,\mathrm{nC\,m^{-3}}$), the SP98 scheme resulted in a normal tripole charge structure (Fig. 12). A simple normal dipole charge structure also occur in some of the storm cells forming the rainbands (see Fig. 12 at $\mathrm{X} = 450$ km).

Almost all of the CG flashes produced in the eyewall of the storm were $-$CG flashes (i.e., they lowered negative charge to the surface). The majority of the $-$CG flashes were found radially outside the eyewall on the northwestern side (Fig. 6). Note that the rainbands were essentially

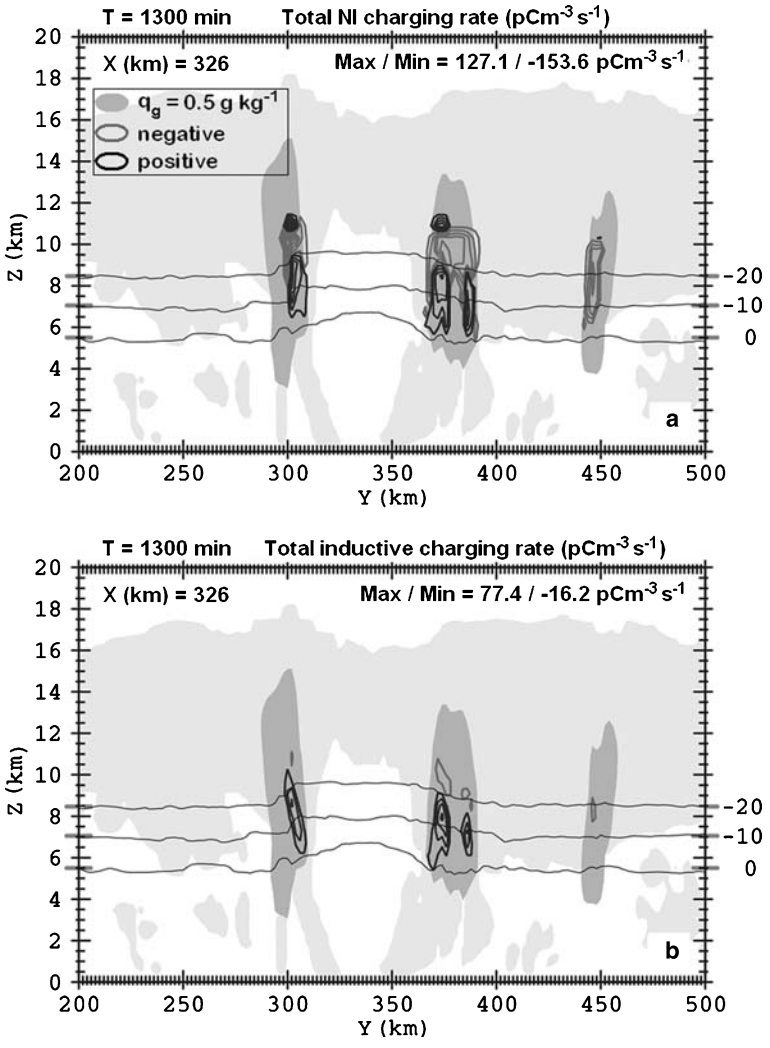

Fig. 13. As in Fig. 10, but for (**a**) total non-inductive, and (**b**) total inductive charging rate in $\mathrm{pC\,m^{-3}\,s^{-1}}$. Positive (negative) contours are shown by the red (blue) contours in increments of $20\,\mathrm{pC\,m^{-3}\,s^{-1}}$ starting at $10\,\mathrm{pC\,m^{-3}\,s^{-1}}$ ($-10\,\mathrm{pC\,m^{-3}\,s^{-1}}$). Darker grey area shows total graupel mixing ratio of $0.5\,\mathrm{g\,kg^{-1}}$ (see legend)

devoid of CG flashes, with the exception of one lone +CG flash. In Fig. 6, the −CG flashes in the eyewall near the vertical cross section shown in Fig. 12, were coincident with a region of larger positive charge density below 6 km. The lone +CG flash in the outer band, however, was coincident with a region of larger negative charge density below 6 km.

To investigate the origins of the charge regions in the storm in more detail, a single cross section at a particular time was selected for the analysis. Similar cross sections across the eyewall were also made a few grid points away and revealed little qualitative difference in the charge and charging structure of the storm at that time. The lower positive charge region (below 7 km) closer to the center of the eyewall (near Y = 300 and Y = 375 km, Fig. 12) was mainly attributed to positive charging of graupel by both the NI and inductive mechanisms (Fig. 13a, b). The main negative charge region located at mid-levels near 8–9 km and the upper positive charge region (near 10 km) were mainly a consequence of NI charging, with a negligible contribution from induction (Figs. 12 and 13a, b).

Between the outer rainbands and the eyewall updrafts, almost no charging was occurring (e.g., Fig. 13, Y = 425 km), since this region of the TC had negligible amounts of CWC and graupel (Fig. 10b). This lack of CWC and graupel between the outer rainbands and the eyewall updrafts was consistent with overall weak updraft speeds ($< 1\,\mathrm{m\,s^{-1}}$ in Fig. 9b). Moreover, this stratiform cloud was essentially glaciated as it was composed almost exclusively of snow particles (Fig. 10a). As a result, most of the charges that are observed in these regions of the storm were likely produced initially in the eyewall convection

and then advected both counterclockwise in azimuth and radially outward by the storm's strong circulation. As charged precipitation particles were advected they fell to lower levels while keeping the polarity of charge gained in the eyewall (see downward slope of the main negative charge region and the upper positive charge region with radial distance away from the eyewall in Fig. 12 between Y = 360 km and Y = 390 km). The three charge layers forming the normal tripole in the eyewall ended at roughly the same radius from the eyewall (Fig. 12), although in some vertical cross sections at earlier times (not shown) the two upper charges regions forming this tripole extended farther into the inner band stratiform region than the lower charge. In this situation, the resulting charge distribution could be described as a normal dipole. The reason for this charge configuration in the inner band region was probably that heavier charged precipitation particles fell out of the lower regions and the remaining mix of hydrometeor types lacked the necessary ingredients for both inductive and NI charging (i.e., there were insufficient concentrations of graupel and ice crystals).

Additional analysis of the charge structure and lightning location at earlier times (not shown) revealed that the maximum in lightning activity in the eyewall was not always near the region of maximum charging. At first, this result may appear counterintuitive. However, while charges must be generated in a region of the eyewall that is more conducive for the NI charging process (because it has a larger CWC and larger total graupel mixing ratio), the advection of these charges by the intense TC circulation can cause the onset of lightning to occur further downwind (similar to the hypotheses of Corbosiero, 1999). In other words, the (strongly sheared) advection and subsequent sedimentation of charges was likely one important factor in determining the lightning distribution in the simulated eyewall.

5. Major issues raised by the hurricane simulations

Once a well-defined eyewall and spiral rainbands started to appear after the initial convective burst near and around the Rankine vortex center, the TC started to lose its definition shortly after 30 h of simulation when the outer rainbands started to expand to form locally strong small storm clusters. At about 35 h of simulation, the bands and cluster of storms that once formed the rainbands have almost completely propagated away from the eyewall. At the same time, the eyewall lost its closed circular characteristic and became progressively more dominated by downdrafts near the melting level. However, the detrimental effect of the low θ_e air from cold pools generated in the outer rainbands did not seem to be the primary cause for the apparent weakening of the eyewall convection. Instead, further analysis showed that the regions devoid of convective activity and surrounding the eyewall at the LCL (between 1 and 1.7 km) were characterized by warm temperature anomalies exceeding 2–3 K which were not present at earlier times (about 5 hours earlier, not shown). The exact reasons behind this warming are still unclear and remain the subject for future work. Since the model did not feature radiation processes, it was possible that the inclusion of a radiative cooling parameterization (e.g., Newtonian cooling) could have helped in minimizing this generalized warming of the atmosphere as the radiative cooling acts on the same time scale as the simulated warming.

Surprisingly, even though the eyewall convection weakened and became more ill-defined, the TC was still undergoing slow progressive deepening. This result appeared counterintuitive, as one would have expected a rapid increase of the central pressure instead. Additional cross sections revealed that the strong warm anomaly caused by subsidence in the eye (and responsible for the pressure fall at the surface in the eye) persisted for several hours after the convection in the eyewall had significantly weakened (not shown). The physical mechanisms causing this behavior of the model remain the subject of future investigation.

6. Conclusions

Using a numerical model featuring a sophisticated 12-class microphysics scheme and a three dimensional lightning module, a high-resolution simulation of a hurricane-like vortex was carried out with success. At about 22 h of simulation, the model reproduced many of the features observed

in TCs in nature. One feature was a well-defined eye and eyewall with several connecting rainbands. Also, the vertical reflectivity and wind profile showed an outward tilt with height that was consistent with a strong mid-level warming aloft caused by adiabatic compression of subsiding air in the eye. This in turn was responsible for the rapid pressure drop at the storm's center via hydrostatic balance. Relatively higher θ_e values were found in the sloping eyewall and in the lowest kilometer inside the eye, which generally agreed with observations.

The largest updraft speeds and resulting total graupel mixing ratios, CWC, and lightning flash rates were found in the eyewall, and within some isolated stronger convective cells forming the outer rainbands. The eyewall updraft speeds at that time were somewhat stronger and deeper than typically observed within mature TCs, which supported the development of more graupel than is typically observed. The outer eyewall stratiform region was mainly composed of lighter ice crystals and snow aggregates that were ejected from the eyewall convection, a pattern which was consistent with observations and also with a dearth of lightning activity there.

The overall charge structure in the eyewall broadly resembled a normal tripole, while in some of the strongest cells in the rainbands and in some portion of the outer eyewall stratiform region a normal dipole was observed. The mid-level negative and upper positive charge layers were mainly a consequence of NI charging while the lowest positive charge region was attributed to both induction and NI charging. This charge configuration across the storm was consistent with almost all ground flashes lowering negative charge to the surface, as in most continental storms.

Acknowledgments

We thank the Office of Naval Research (ONR) for generously sponsoring Alexandre Fierro (grant no. N00014-02-1-0181) for two years and the Oklahoma Supercomputing Center for Education and Research (OSCER) for providing computing resources. We also would like to thank the anonymous reviewers for providing helpful suggestions on an earlier version of the manuscript and also Frank Marks, John Gamache, John Molinari, Robert Rogers and Robert Black for their useful comments. Partial support for this research was also provided by the National Science Foundation under grants ATM-0451639 and ATM-0340693.

References

Anderson JR, Droegemeier KK, Wilhelmson RB (1985) Simulation of the thunderstorm sublcoud environment. Preprints, 14th Conf. on Severe Local Storms, Indianapolis, Amer Meteor Soc, pp 147–150

Bedrick M, Burgett W (1999) A tropical oceanic cloud-to-ground lightning study. Preprints, 23rd Conf. on Hurricanes and Tropical Meteorology, Dallas, Amer Meteor Soc, pp 243–245

Black ML, Burpee RW, Marks FD (1996) Vertical motion characteristics of tropical cyclones determined with airborne Doppler radial velocities. J Atmos Sci 53: 1887–1909

Black PG, Black RA, Hallett J, Lyons WA (1986) Electrical activity of the hurricane. Preprints, 23rd Conf. on Radar Meteorology, Snowmass, Amer Meteor Soc, pp J277–J280

Black RA (1984) Distribution of particles types above 6.0 km in two Atlantic hurricanes. Preprints, 16th Conf. on Hurricanes and Tropical Meteorology, San Diego, Amer Meteor Soc, pp 537–541

Black RA, Hallett J (1986) Observations of the distribution of ice in hurricanes. J Atmos Sci 43: 802–822

Black RA, Hallett J (1990) Electric field and microphysical measurements in vigorous hurricane eyewalls. Preprints, Conf. on Cloud Physics, San Francisco, Amer Meteor Soc, pp 662–665

Black RA, Hallett J (1999) Electrification of the hurricane. J Atmos Sci 56: 2004–2028

Black RA, Hallett J, Saunders CPR (1993) Aircraft studies of precipitation and electrification in hurricanes. Preprints, 17th Conf. on Severe Local Storms, St. Louis, Amer Meteor Soc, pp J20–J25

Black RA, Bluestein HB, Black ML (1994) Unusually strong vertical motions in a Caribbean hurricane. Mon Wea Rev 122: 2722–2739

Black RA, Hallett J, Willis P (1995) Aircraft measurements of ice and electrical evolution in regions of vertical shear in convective cloud. 21st General Assembly of IUGG, Boulder, Co

Bister M, Emanuel KA (1998) Dissipative heating and hurricane intensity. Meteorol Atmos Phys 65: 233–240

Blackwell KG (2000) The evolution of hurricane Danny (1997) at landfall: Doppler-observed eyewall replacement, vortex contraction/intensification and low-level wind maxima. Mon Wea Rev 128: 4002–4016

Boccippio DJ, Cummins KL, Christian HJ, Goodman SJ (2001) Combined satellite- and surface-based estimation of the intracloud-cloud-to-ground lightning ratio over the continental United States. Mon Wea Rev 129: 108–122

Braun SA (2002) A cloud-resolving simulation of hurricane Bob (1991): Storm structure and eyewall buoyancy. Mon Wea Rev 130: 1573–1592

Brooks IM, Saunders CPR, Mitzeva RP, Peck SL (1997) The effect on thunderstorm charging of the rate of rime accretion by graupel. J Atmos Res 43: 277–295

Bryan GH, Wyngaard JC, Fritsch JM (2003) Resolution requirements for the simulation of deep moist convection. Mon Wea Rev 131: 2394–2416

Carey LD, Rutledge SA (1998) Electrical and multiparameter radar observations of a severe hailstorm. J Geophys Res 103: 13979–14000

Cecil DJ, Zipser EJ, Nesbitt SW (2002a) Reflectivity, ice scattering, and lightning characteristics of hurricane eyewalls and rainbands. Part I: Quantitative description. Mon Wea Rev 130: 769–784

Cecil DJ, Zipser EJ, Nesbitt SW (2002b) Reflectivity, ice scattering, and lightning characteristics of hurricane eyewalls and rainbands. Part II: Intercomparison of observations. Mon Wea Rev 130: 785–801

Chiu CS (1978) Numerical study of cloud electrification in an axisymmetric, time-dependent cloud model. J Geophys Res 81: 5025–5049

Corbosiero KL (1999) Lightning in hurricanes. Preprints, 23rd Conf. on Hurricanes and Tropical Meteorology, Dallas, Amer Meteor Soc, pp 66–67

Cummings KL, Murphy MJ, Bardo EA, Hiscox WL, Pyle RB, Pifer AE (1998) A combined TOA/MDF technology upgrade of the U.S. National Lightning Detection Network. J Geophys Res 103 (D8): 9035–9044

Deardroff JW (1980) Stratocumulus-capped mixed layers derived from a three-dimensional model. Bound-Layer Meteor 18: 495–527

Demetriades NWS, Holle RL (2005) Long-range lightning applications for hurricane intensity and precipitation nowcasting. Preprints, Conf. Meteorology Application of Lightning Data, San Diego, Amer Meteor Soc, 9 pp

Demetriades NWS, Holle RL (2006) Long-range lightning nowcasting applications for tropical cyclones. Preprints, Conf. Meteorology Application of Lightning Data, Atlanta, Amer Meteor Soc, 9 pp

Eastin MD (1999) Evaluation of buoyant motions within the hurricane inner core. Preprints, 23rd Conf. on Hurricanes and Tropical Meteorology, Dallas, Amer Meteor Soc, pp 91–94

Emanuel KA (1986) An air-sea interaction theory for tropical cyclone. Part I: Steady state maintenance. J Atmos Sci 43: 585–604

Fierro AO, Gilmore MS, Mansell ER, Wicker LJ, Straka JM (2006) Electrification and lightning in an idealized boundary-crossing supercell simulation of 2 June 1995. Mon Wea Rev 134: 3149–3172

Fiorino M, Elsberry RL (1989) Some aspects of vortex structure related to tropical cyclone motion. J Atmos Sci 46: 975–990

Gardiner B, Lamb D, Pitter RL, Hallet J, Saunders CPR (1985) Measurements of initial potential gradient and particles charges in a Montana thunderstorm. J Geophys Res 90: 6079–6086

Gilmore MS, Wicker LJ (1998) The influence of midtropospheric dryness on supercell morphology and evolution. Mon Wea Rev 126: 943–958

Goodman SJ, MacGorman DR (1986) Cloud-to-ground lightning activity in mesoscale convective complexes. Mon Wea Rev 114: 2320–2328

Gray WM (1995) Tropical Cyclones. Report, World Meteor Org, 163 pp

Halverson J, Azofeifa PL, Black M, Braun S, Cecil D, Goodman M, Heymsfield A, Heymsfield G, Hood R, Krishnamurti T, McFarquhar G, Molinari J, Rogers R, Turk J, Velden C, Zhang DL, Zipser E, Kakar R (2006) NASA's Tropical Cloud Systems and Processes (TCSP) Experiment: Investigating Tropical Cyclogenesis and Hurricane Intensity Change. Submitted to Bull Amer Meteor Soc

Helsdon JH, Wojcik WA, Farley RD (2001) An examination of thunderstorm-charging mechanisms using a two-dimensional storm electrification model. J Geophys Res 106: 1165–1192

Heymsfield GM, Bidwell S, Caylor IJ, Ameen S, Nicholson S, Boncyk W, Miller L, Vandemark D, Racette PE, Dod LR (1996) The EDOP radar system on the high-altitude NASA ER-2 aircraft. J Atmos Oceanic Tech 13: 795–809

Jorgensen DP, Zipser EJ, LeMone MA (1985) Vertical motions in intense hurricanes. J Atmos Sci 42: 839–856

Kanak KM (1990) Three-dimensional, non-hydrostatic, numerical simulation of a developing tropical cyclone. M.S. Thesis, University of Wisconsin, pp 130

Kelley OA, Stout J, Halverson JB (2004) Tall precipitation cells in tropical cyclone eyewalls are associated with tropical cyclone intensification. Geophys Res Lett 31: L24112–L24115

Kessler E (1969) On the distribution and continuity of water substance in atmospheric circulation. Meteor Monog, Amer Meteor Soc, 84 pp

Kuhlman KM, Ziegler CL, Mansell ER, MacGorman DR, Straka JM (2006) Numerical simulations of the 29 June 2000 STEPS supercell: microphysics, electrification, and lightning. Mon Wea Rev 134: 2734–2757

Lang TJ, Rutledge SA (2002) Relationships between convective storm kinematics, precipitation, and lightning. Mon Wea Rev 130: 2492–2506

Leonard BP (1991) The ultimate conservative difference scheme applied to unsteady one-dimensional advection. Comput Methods Appl Mech Eng 88: 17–74

Lhermitte RM, Krehbiel P (1979) Doppler radar and radio observations of thunderstorms. IEEE Trans Geosci Electron 17: 162–171

Louis JF (1979) A parametric model of vertical eddy fluxes in the atmosphere. Bound-Layer Meteor 17: 187–202

Lyons WA, Venne MG, Black PG, Gentry RC (1989) Hurricane lightning: A new diagnostic tool for tropical storm forecasting? Preprints, 18th Conf. on Hurricanes and Tropical Meteorology, San Diego, Amer Meteor Soc, pp 113–114

MacGorman DR, Nielsen KE (1991) Cloud-to-ground lightning in a tornadic storm on 8 May 1986. Mon Wea Rev 119: 1557–1574

MacGorman DR, Rust WD (1998) The electrical nature of storms. Oxford University Press, New York, 422 pp

MacGorman DR, Burgess DW, Mazur V, Rust WD, Taylor WL, Johnson BC (1989) Lightning rates relative to tornadic storm evolution on 22 may 1981. J Atmos Sci 46: 221–250

Mansell ER, MacGorman DR, Ziegler CL, Straka JM (2002) Simulated three-dimensional branched lightning in a numerical thunderstorm model. J Geophys Res 107: D9 (doi: 10.1029/2000JD000244)

Mansell ER, MacGorman DR, Ziegler CL, Straka JM (2005) Charge structure and lightning sensitivity in a simulated multicell storm. J Geophys Res 110: D12101 (DOI: 10.1029/2004JD005287)

McFarquhar GM, Black RA (2004) Observations of particle size and phase in tropical cyclones: Implications for mesoscale modeling of microphysical processes. J Atmos Sci 61: 422–439

Meyers MP, DeMott PJ, Cotton WR (1992) New primary ice-nucleation parameterizations in an explicit cloud model. J Appl Meteor 31: 708–721

Molinari J, Moore PK, Idone VP, Henderson RW, Saljoughy AB (1994) Cloud-to-ground lightning in Hurricane Andrew. J Geophys Res-Atmos 99: 16665–16676

Molinari, J, Moore PK, Idone VP (1999) Convective structure of hurricanes as revealed by lightning locations. Mon Wea Rev 127: 520–534

Morales CA, Kriz JS (1997) The evolution of sferics around hurricane Lilli-1996. Preprints, 22nd Conf. on Hurricanes and Tropical Meteorology, Ft. Collins, Amer Meteor Soc, pp 127–128

Orville RE, Coyne JM (1999) Could-to-ground lightning in tropical cyclones (1986–1996). Preprints, 23rd Conf. on Hurricanes and Tropical Meteorology, Dallas, Amer Meteor Soc, 194 pp

Petersen WA, Cifelli RC, Rutledge SA, Ferrier BS, Smull BF (1999) Shipborne dual-Doppler operations and observations during TOGA COARE. Bull Amer Meteor Soc 80: 81–97

Reap RM, MacGorman DR (1989) Cloud-to-ground lightning: Climatological characteristics and relationships to model fields, radar observations, and severe local storms. Mon Wea Rev 117: 518–535

Rodgers E, Weinman J, Pierce H, Olson W (2000) Tropical cyclone lightning distribution and it relationship to convection and intensity change. Preprints, 24th Conf. on Hurricanes and Tropical Meteorology, Ft. Lauderdale, Amer Meteor Soc, pp 537–541

Rogers FR, Black ML, Chen SS, Black RA (2006) An evaluation of microphysical fields from mesoscale model simulation of tropical cyclones. Part I: Comparisons with observations. J Atmos Sci (submitted)

Rotunno R, Emanuel KA (1987) An air-sea interaction theory for tropical cyclones. Part II: evolutionary study using a nonhydrostatic axisymmetric numerical model. J Atmos Sci 44: 542–561

Rutledge SA, MacGorman DR (1988) Cloud-to-ground lightning activity in the 10–11 June 1985 mesoscale convective system observed during the Oklahoma-Kansas PRE-STORM Project. Mon Wea Rev 116: 1393–1408

Rutledge SA, Williams ER, Keenan TD (1992) The down under doppler and electricity experiment (DUNDEE): Overview and preliminary results. Bull Amer Meteor Soc 73: 3–16

Samsury CE, Orville RE (1994) Cloud-to-ground lightning in tropical cyclones: a study of hurricanes Hugo (1989) and Jerry (1989). Mon Wea Rev 122: 1887–1896

Saunders CPR, Peck LS (1998) Laboratory studies of the influence of the rime accretion rate on charge transfer during crystal/graupel collisions. J Geophys Res 103: 13949–13956

Schubert WH, Hack JJ (1982) Inertial stability and tropical cyclone development. J Atmos Sci 39: 1687–1697

Shao XM, Harlin J, Stock M, Stanley M, Regan A, Wiens K, Hamlin T, Pongratz M, Suszcynsky D, Light T (2005) Katrina and Rita were lit up with lightning. Eos 86(42), 18 October

Simpson RH (1974) The hurricane disaster potential scale. Weatherwise 27: 169–186

Straka JM, Mansell ER (2005) A bulk microphysics parameterization with multiple ice precipitation categories. J Appl Meteor 44: 445–466

Takahashi T (1978) Riming electrification as a charge generation mechanism in thunderstorms. J Atmos Sci 35: 1536–1548

Tremback CJ, Powell J, Cotton WR, Pielke RA (1987) The forward-in-time upstream advection scheme: extension to higher orders. Mon Wea Rev 115: 540–555

Velden C, Hayden CM, Menzel WP, Franklin JL, Lynch JS (1992) The impact of satellite-derived winds on numerical hurricane track forecasting. Wea Forecast 7: 107–118

Wang Y (2002) An explicit simulation of tropical cyclones with a triply nested movable mesh primitive equation model: TCM3. Part II: Model refinements and sensitivity to cloud microphysics parameterization. Mon Wea Rev 130: 3022–3036

Wiens KC, Rutledge SA, Tessendorf SA (2005) The 29 June 2000 Supercell observed during steps. Part II: Lightning and charge structure. J Atmos Sci 62: 4151–4177

Williams ER (1989) The tripole structure of thunderstorms. J Geophys Res 94: 13151–13167

Willis PT, Heymsfield AJ (1989) Trajectories of hydrometeors in hurricane Emily. Preprints, 16th Conf. on Hurricanes and Tropical Meteorology. San Diego, Amer Meteor Soc, pp 192–196

Willoughby HE (1998) Tropical cyclone eye thermodynamics. Mon Wea Rev 126: 3053–3067

Zehnder JA, Reeder MJ (1997) A numerical study of barotropic vortex motion near large scale mountain ranges with application to the motion of tropical cyclones approaching the Sierra Madre. Meteorol Atmos Phys 64: 1–19

Zhu H, Smith RK (2002) The importance of three physical processes in a three-dimensional tropical cyclone model. J Atmos Sci 59: 1825–1840

Ziegler CL, MacGorman DR, Dye JE, Ray PS (1991) A model evaluation of non-inductive graupel-ice charging in the early electrification of a mountain thunderstorm. J Geophys Res 96: 12833–12855

Zrnic DS, Balakrishnan N, Ziegler CL, Bringi VN, Aydin K, Matejka T (1993) Polarimetric signatures in the stratiform region of a mesoscale convective system. J Appl Meteor 32: 678–693

Corresponding author's address: Alexandre O. Fierro, School of Meteorology, University of Oklahoma, National Weather Center, 120 David L. Boren Blvd. Suite 5900 Norman, OK 73072-7307, USA (E-mail: afierro@ou.edu)